Adsorption and Thermal Decomposition Chemistry of 1-Propanol and Other Primary Alcohols on the Si(100) Surface

Linhu Zhang, April J. Carman, and Sean M. Casey*

Department of Chemistry and Chemical Physics Program, MS 216, University of Nevada, Reno, Nevada 89557

Received: August 22, 2002; In Final Form: May 5, 2003

The adsorption of several simple primary alcohols (1-propanol, ethanol, and methanol) on the Si(100)−(2 × 1) surface has been investigated using Auger electron spectroscopy (AES) and thermal desorption spectroscopy (TDS). These alcohols appear to undergo dissociative adsorption on this surface at room temperature. These results are in agreement with infrared and photoemission spectroscopic studies of ethanol and methanol adsorption. By comparison to the AES results from the adsorption of methyl iodide on Si(100), it was concluded that the surface saturation coverage of 1-propanol on Si(100) is slightly less than half a monolayer, identical (within experimental uncertainty) to the saturation coverages of ethanol and methanol. TDS reveals no parent desorption channels for all three of these molecules, and instead provides evidence for a β-hydrogen elimination channel of the surface-bound alkoxy radicals, as well as competing surface decomposition channels. To gain further physical insight into the available reaction pathways for these molecules on this surface, we have used ab initio and density functional theories to study adsorption on silicon clusters and found that the reaction paths obtained from this computational treatment are consistent with the experimental results.

I. Introduction

Silicon surface chemistry has received extensive attention in the past, and continues to be the focus of much study because of this material's importance to modern science and technology.[1−7] Silicon surface reactivity is dependent on the electronic environment of the surface atoms (i.e., the dangling bonds), which is governed by the geometrical arrangement of the atoms at the surface. The (100) surface of silicon, for example, undergoes a 2 × 1 reconstruction, resulting in the formation of rows of silicon surface dimers.[8−11] The silicon atoms in these surface dimers are bound to each other by a relatively strong σ-type bond and a weak π-type bond, and each atom in the dimer is also bound to two other silicon atoms underneath it in the bulk.

These dimers have been observed to undergo facile addition-type reactions with active hydrogen compounds such as hydrogen halides,[12−14] alcohols,[15−20] and water,[21−24] as well as with amines[25−33] and phosphines.[34−36] In the case of amines, the initial interaction with the surface is thought to occur via a nucleophilic attack by the nitrogen lone-pair on one of the silicon atoms in the dimer.[31−33] The surface dimers can accommodate this type of interaction in their buckled form, which has an electron distribution that is shifted from the π-like orbital of the symmetric dimer to a zwitterionic-type distribution with the lower silicon atom of the buckled pair having a partial positive charge and the upper atom having a partial negative charge. The partial positive charge on the lower silicon atom stabilizes the "dative bond" resulting from the nucleophilic attack of the nitrogen lone-pair on this atom. Further reaction with the surface can then occur, for primary and secondary amines, by hydrogen transfer to the electronegative, upper silicon atom of the buckled dimer. Tertiary amines, which do not have this channel available, can become trapped in the dative-bond well, forming a quaternary ammonium-type adduct.[31−33] A similar reaction through a trivalent oxygen atom is thought to occur for methanol interactions with these surface dimers.[16,17] Previous photoemission and infrared spectroscopic studies on ethanol[19,20] and methanol[15,18] adsorption on this surface provide evidence of ethoxy and methoxy formation after adsorption, consistent with this addition reaction mechanism. Some evidence exists for C−O bond cleavage in methanol at high surface coverages,[18] although the mechanisms for these reactions are currently not entirely clear.

In this study, the adsorption and reactions of 1-propanol, ethanol, and methanol are compared on the Si(100)−(2 × 1) surface using Auger electron spectroscopy (AES), thermal desorption spectroscopy (TDS), and ab initio and density functional theory (DFT)[37,38] computations in order to further probe the reactivity of alcohols on this surface. Thermal desorption reveals that decomposition on this surface during heating to form volatile aldehydes is a common reaction for these primary alcohols. Results from these studies complement the photoemission,[18,20] reflection infrared spectroscopic,[15,19] and computational studies[16,17] that have been reported on these systems and provide further detail about the energetics of these surface reactions.

II. Experimental and Computational Methods

The alcohol adsorption and decomposition experiments were carried out in a stainless steel ultrahigh vacuum (UHV) chamber that has been described in detail elsewhere.[30] The chamber is equipped with rear-view four-grid low-energy electron diffraction (LEED) optics that are utilized in retarding-field analysis mode for the recording of Auger electron spectra. The chamber is also equipped with a cold-cathode argon ion gun for sample cleaning and a quadrupole mass spectrometer (QMS) for residual gas analysis and for thermal desorption studies. The Si(100) single-crystal wafers (arsenic-doped, 1−20 Ω cm, ± 0.5°) used in this work were 0.4−0.6-mm thick and were mechanochemi-

* Corresponding author. Phone: (775) 784-4133. Fax: (775) 784-6804. E-mail: scasey@chem.unr.edu.

10.1021/jp021942o CCC: $25.00
Published on Web 07/24/2003

cally mirror polished on one side (Polishing Corporation of America). Prior to introduction into the chamber, samples were cut to about 2.5 cm^2 and were cleaned by utilizing a series of argon sputtering and annealing cycles. The surface structure and cleanliness after the cleaning cycles were confirmed using LEED and AES. Sample temperatures were measured using a tungsten−5% rhenium vs tungsten−26% rhenium (type-C) thermocouple junction spot-welded to the tantalum backing plate immediately adjacent to the sample. Temperatures were also calibrated against desorption temperatures for the H_2 and SiO desorption products from adsorption of water,[39] H_2 and NH_3 desorption products from ammonia adsorption,[25] and H_2 and C_4H_8 desorption products from the adsorption of *cis*-2-butene on the Si(100) surface.[40] The methanol (Fisher, 99.8%), ethanol (Pharmco, 99.5%), and 1-propanol (Acros, 99.5%) samples that were used in these studies were all subjected to several (at least three) freeze−pump−thaw cycles prior to introduction into the vacuum chamber via a variable stainless steel leak valve. All doses were performed with the sample held in the 300−350 K temperature range unless otherwise noted. Exposures are reported in Langmuirs (1 L = 1×10^{-6} Torr s), using the uncorrected pressure reading from a nude ion gauge located in the UHV chamber.

To gain further physical insight into the available reaction pathways for these molecules on the Si(100) surface, we have used ab initio molecular orbital calculations along with DFT to study alcohol physisorption and chemisorption on Si_9H_{12} single-dimer silicon clusters.[41] The ab initio molecular orbital calculations were carried out on these systems at the Hartree−Fock (HF) level of theory[42] for geometry optimizations using the Gaussian 98 program package.[43] None of the geometrical parameters describing the cluster or adsorbate were fixed during the optimization calculations. The basis sets for these calculations were double-ζ Gaussian-type basis sets with polarization functions added to the heavy atoms [the 3-21G(d) basis set, in Gaussian notation].[44−48] Vibrational frequencies were calculated[49,50] at this level of theory for optimized minima and transition states in order to verify the assignment of these stationary points. The intrinsic reaction coordinates (IRCs)[51,52] between the transition states and the minima were mapped either by fixing the positions of all of the cluster atoms except for the "surface dimer" and the adsorbate at their transition state values, or by allowing all atoms to relax. The result from the first approach is convergence of the reaction coordinate calculation to a stationary point that is higher in energy than the true, relaxed-cluster minimum; however, this comes at a greatly reduced computational effort. Adsorption (following the free molecule + cluster into the molecularly adsorbed well) reaction coordinates were followed by fixing the approach angles of the molecule to be close to normal to the surface dimer. Single-point energies for minima and transition states were calculated at the HF optimized geometries using DFT at the B3LYP level of theory[53,54] and using triple-ζ basis sets with diffuse and polarization functions added to heavy atoms and polarization functions added to hydrogen atoms [the 6-311+G(2d,p) basis set, in Gaussian notation].[55−57] Zero-point vibrational corrections were made to all reported single-point energies.

III. Results and Discussion

A. Computations. Figure 1 shows a schematic potential energy curve from the computational results for the interaction of the 1-propanol molecule with a silicon cluster that is meant to model the Si(100)−(2 × 1) surface, as is outlined in Section II, above. The 1-propanol molecule initially interacts with the silicon surface dimer through the formation of a "dative" bond,

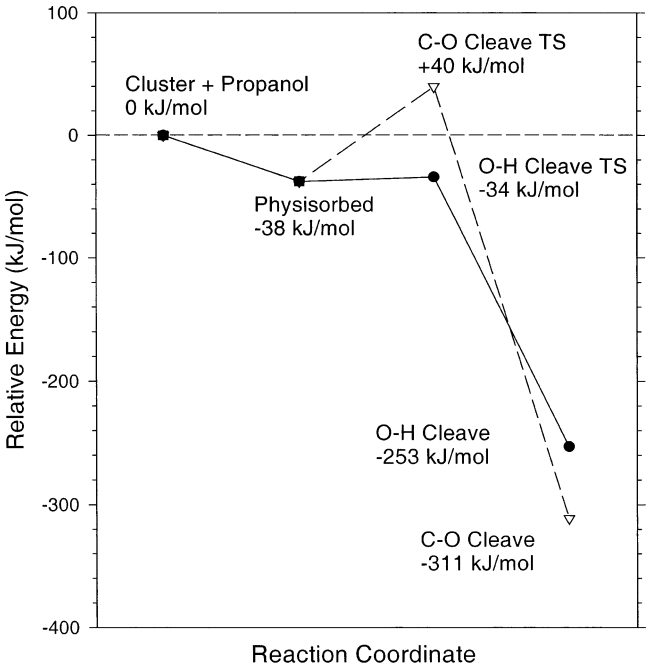

Figure 1. Schematic diagram showing the relative energy levels of the 1-propanol molecule interacting with a Si_9H_{12} cluster obtained using the computational methods outlined in Section II of the text. The relative energies along the O−C and O−H cleavage reaction paths are depicted.

which occurs with no barrier as the incident gas-phase propanol molecule approaches the surface. This is similar in nature to the predicted initial interaction of the water[22] and methanol[16,17] molecules with this surface. Once in the "physisorbed," datively bonded well, propanol can proceed to react with the surface via a number of pathways. Two of these reaction paths are shown schematically in Figure 1: O−H bond cleavage and O−C bond cleavage. The geometries for the stationary points along this path are shown in Figure 2. Additional reaction pathways that are available to the 1-propanol molecule include α-C−H bond cleavage, β-C−H bond cleavage, and γ-C−H bond cleavage. Figure 3 shows a schematic potential energy curve for these three reaction paths, while the geometries for the stationary points along this path are shown in Figure 4. Table 1 presents the computed values for all of these reactions paths for the 1-propanol molecule on the Si_9H_{12} cluster, along with results for the related ethanol molecule, which has the same pathways (with the exception of the γ-C−H bond cleavage pathway) available to it, and results for methanol, which has no γ-C−H bond cleavage or β-C−H bond cleavage path. For comparison, the table also presents available previously computed values[16,17] for these reaction coordinates. The stationary point energy values computed for methanol using the methods outlined in section II are in agreement with results from more extensive computational approaches,[16,17] with the exception of the value for the dative-bond well. This value appears to be low compared to the more extensive theoretical calculations, by about 25 kJ/mol, and it is likely that the values for this well presented in Table 1 for ethanol and 1-propanol are also underestimated by a similar amount. It is also likely that agreement would be improved by using a larger dimer cluster model to account for any charge delocalization or surface relaxation that may be important for accommodation of this dative bond by the surface.[29,33]

Table 1 shows that for all of these molecules any of the reaction paths out of the dative-bond well have significant (at least 55 kJ/mol) barriers to reaction, when measured from the bottom of this well, except for O−H bond cleavage, which

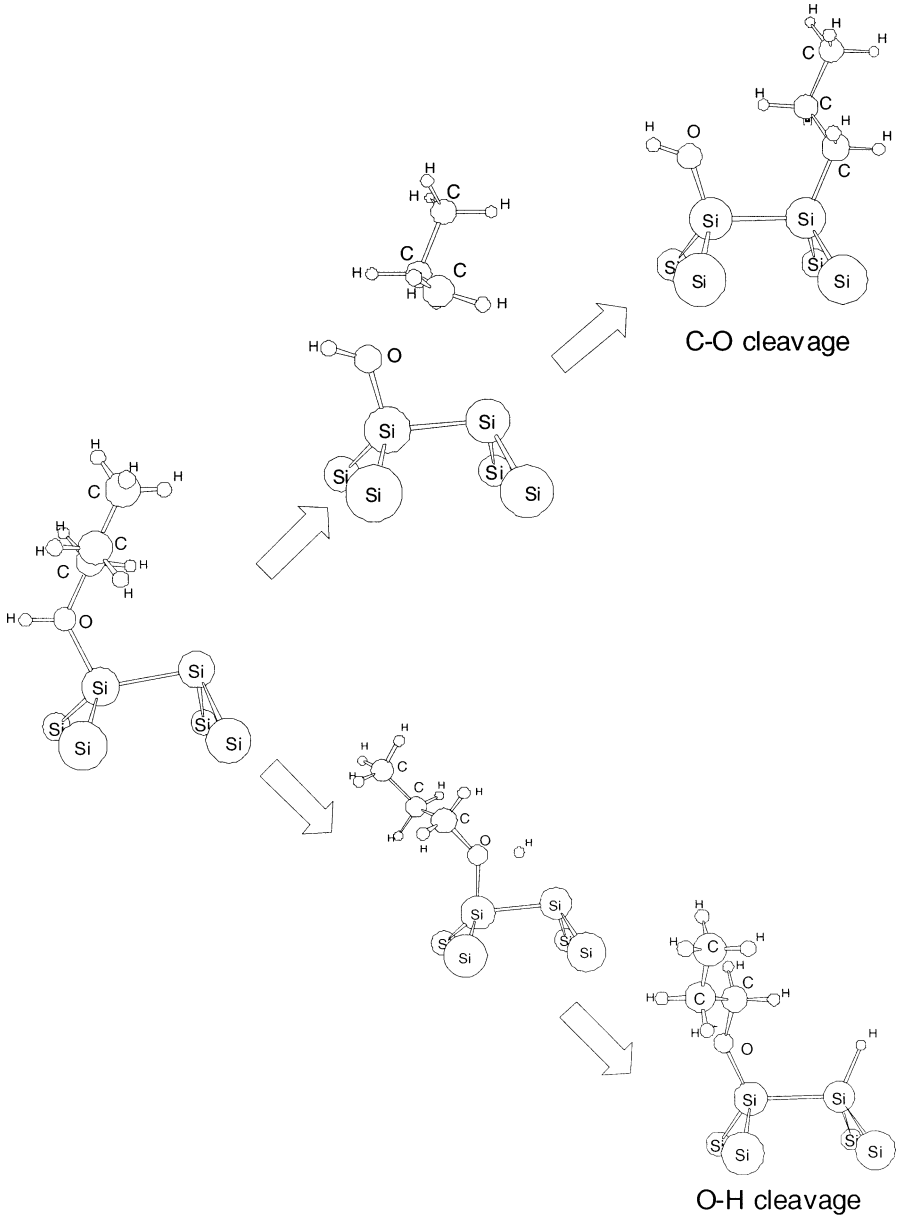

Figure 2. Geometries of the stationary points along the 1-propanol/Si_9H_{12} reaction paths displayed in Figure 1. These geometries are the results of the computations described in Section II of the text. Only the top six atoms of the Si_9H_{12} cluster are shown (along with the adsorbate) for clarity.

appears to have a barrier of only 3−17 kJ/mol.[58] This O−H bond cleavage barrier is calculated to be below the initial energy of a free molecule and a bare cluster for all three of the alcohols studied here, while the other barriers, for O−C bond cleavage and for the C−H bond cleavage channels, are all above this level. The ordering of the O−C and O−H bond cleavage channels has previously been noted in the case of methanol,[17] and can rationalize infrared[15] and photoemission[18] results which indicate surface-bound methoxy species upon methanol adsorption on this surface.

For all of these alcohols, O−C bond cleavage appears to be the thermodynamically favored final product, followed by O−H bond cleavage, and finally, the various C−H bond cleavage products. However, as mentioned above, the O−C bond cleavage reaction path has a much higher barrier to overcome than the O−H bond cleavage channel, making O−H bond cleavage the kinetically favored reaction route. Inclusion of the possible C−H bond cleavage channels does not appear to alter this energetic ordering. In fact, on the basis of the computational results presented in Table 1, the C−H bond cleavage channels modeled on the Si_9H_{12} single-dimer cluster are less favorable than the O−H bond cleavage reaction channel both kinetically (higher barriers) and thermodynamically (shallower wells) and also appear to be generally less favorable than O−C bond cleavage, although the β-C−H bond cleavage channel appears to be kinetically favorable compared to the O−C bond cleavage reaction path, for both ethanol and 1-propanol. The high barrier for C−H bond cleavage is somewhat surprising on the basis of the ease of hydrogen transfer for O−H bond cleavage. However, the chemistry of these reaction paths is quite different, as has been noted for the similar case of methylamine reacting with this surface.[33] In the case of methylamine, the N−H bond cleavage reaction has a transition state that basically involves a proton transfer between the quaternary ammonium-like nitrogen atom (formal charge +1) in its datively bound state to the electron-rich, nucleophilic "up" silicon atom (formal charge −1) of the dimer.[59] The result is a reduction of the formal charges during and after hydrogen transfer. The situation is likely to be very similar for alcohols, which have tertiary-bound oxygen atoms in the dative-bond well; this comparison has been made

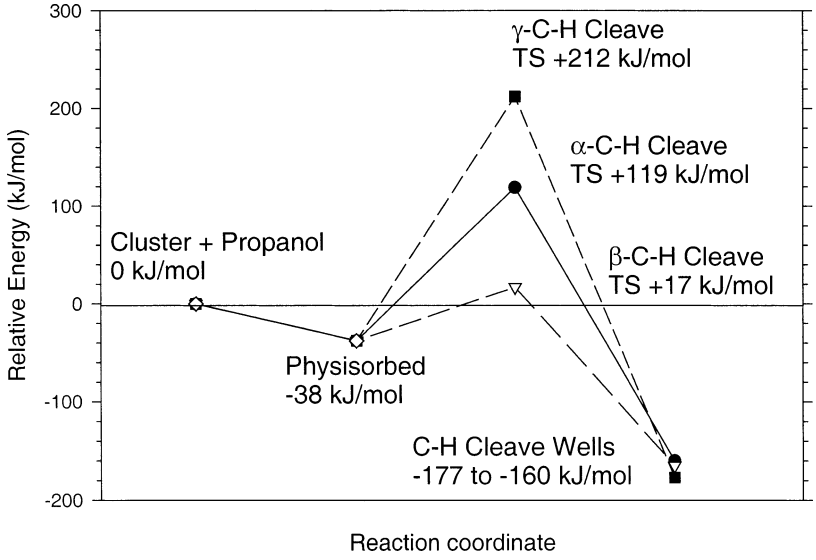

Figure 3. Schematic diagram showing the relative energy levels of the 1-propanol molecule interacting with a Si_9H_{12} cluster obtained using the computational methods outlined in Section II of the text. The relative energies along the three C−H cleavage reaction paths are depicted.

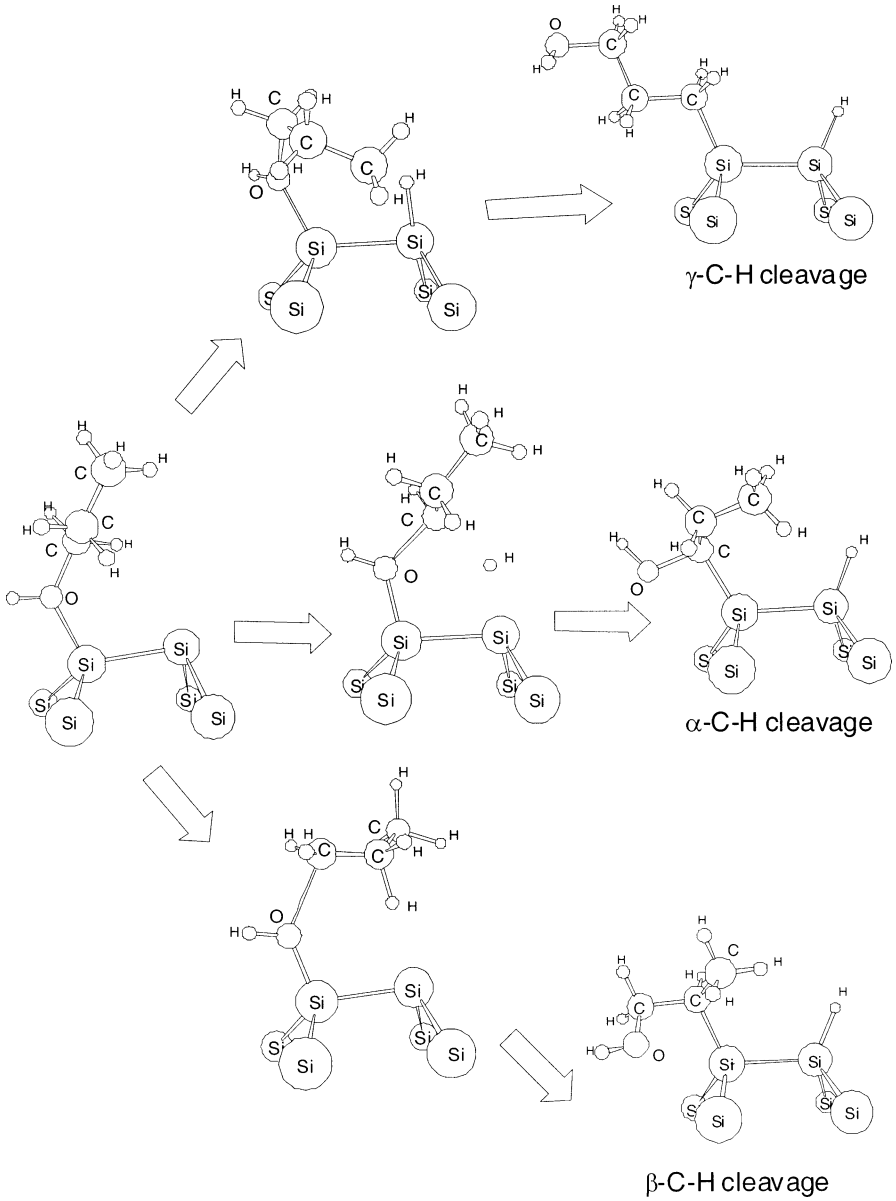

Figure 4. Geometries of the stationary points along the 1-propanol/Si_9H_{12} reaction paths displayed in Figure 3. These geometries are the results of the computations described in Section II of the text.

TABLE 1: Comparison of Results from the Computational Treatment of Alcohol Adsorption As Described in Section II with Previous Computational Results[a,b]

	Single Dimer (Si_9H_{12}) Values in kJ/mol											
	dative bond well	O−H transition state	O−C transition state #1 (front-side attack)	O−C transition state #2 (inversion)	α-C−H transition state	β-C−H transition state	γ-C−H transition state	O−H well	O−C well	α-C−H well	β-C−H well	γ-C−H well
CH_3OH												
theory[c]	−31	−33	52	103	119	N. A.	N.A.	−255	−336	−168	N.A.	N.A.
Lu et al.[d]	−52	−35	−	−	−			−271	−	−		
Kato et al.[e]	−60	−44	59	−	−			−273	−339	−		
CH_3CH_2OH												
theory[c]	−37	−34	38	−	119	21	N. A.	−252	−310	−164	−161	N.A.
$CH_3CH_2CH_2OH$												
theory[c]	−38	−34	40	−	119	17	212	−253	−311	−160	−165	−177

[a] "N.A." indicates not applicable. [b] "−" indicates not calculated. [c] Results from this work. [d] Ref 16. [e] Ref 17.

elsewhere for the case of methanol.[17] For α-C−H bond cleavage, a proton is transferred to the "up" silicon atom, negating its −1 formal charge, but creating a primary carbanion-like electron distribution around the carbon atom. This "anionic" carbon atom is bonded directly to the tertiary-bound oxygen atom, creating a somewhat unstable zwitterionic species, and causing this reaction channel to have a high barrier. Rearrangement (O−Si bond displacement by the carbon) of this zwitterionic radical species leads to formal charge reduction and the formation of the Si−C and Si−H bonds of the α-C−H bond cleavage well.

The γ-C−H cleavage reaction path appears to follow a similar mechanism, but is destabilized at the transition state relative to the α-cleavage channel. This is likely to be due to the isolated nature of the primary carbanion-like carbon formed in the γ-cleavage case, which is further away from the stabilizing presence of the partially positive oxygen atom than in the α-cleavage case. The β-C−H cleavage reaction path appears to have the lowest barrier of the available C−H cleavage reaction paths, and may be competitive with C−O bond cleavage. The transition state for β-C−H cleavage appears to be stabilized relative to the other C−H cleavage reaction paths by a resonance effect. There is a significant lengthening of the C−O bond in this transition state (to about 2.1 Å compared to 1.7 Å and 1.5 Å for α- and γ-cleavage, respectively). In fact, on the basis of the geometry at this transition state, it appears likely that there would be a competing propylene (or ethylene in the case of ethanol) desorption channel. The intrinsic reaction coordinate along this path does indeed show propylene formation. Once formed, propylene can either insert into the Si−O bond, forming the β-C−H cleavage product, or desorb. The insertion transition state (the second transition state along the β-C−H cleavage reaction path; not depicted in Figure 3) is 216 kJ/mol above the propylene desorption channel (which is calculated to be 231 kJ/mol below the cluster + free propanol asymptote), and is not likely to be competitive with desorption. However, it should be noted that propylene formation via β-C−H bond cleavage still has an initial reaction barrier from the datively bonded well that is predicted to be about 50 kJ/mol higher than the barrier for O−H bond cleavage. Thus, it is likely not to be competitive with the O−H bond cleavage path that is available for these alcohols during the initial, room-temperature interaction. The C−O and β-C−H bond cleavage reaction paths are likely to be much more important to ether reactions on this surface, since no O−H cleavage channel exists in the case of ethers. This prediction is currently under investigation in our laboratory.

The O−C bond cleavage reaction path is predicted to be less energetically costly (by about 32 kJ/mol) in the case of methanol than the N−C bond cleavage path of methylamine.[31,33] This reaction has been postulated to proceed via a nucleophilic attack on the carbon atom by the "up" silicon atom of the dimer in the case of methylamine,[31] and a similar mechanism is likely to apply for the alcohol reactions. The lower barrier in the O−C bond cleavage reaction path is consistent with the idea that the hydroxyl radical is a better "leaving group" than the amino radical. The transition state geometries for this nucleophilic attack in both the methylamine and methanol cases reveal that the attack occurs via a "front-side" insertion geometry— a path that has been shown to be noncompetitive with the "backside," inversion attack for gas-phase S_N2 reactions involving ions.[60] The traditional "backside" attack transition state in the case of methanol lies approximately 51 kJ/mol higher than the front-side geometry (see Table 1), and it is likely to be even higher in the cases of ethanol and 1-propanol due to the increased steric hindrance that the alkyl chains of these molecules introduce. The front-side and backside geometries for O−C bond cleavage in the case of methanol are shown in Figure 5 for clarity. For methylamine, the inversion transition state was also found to be higher in energy than the front-side nucleophilic attack.[33] The flipping in the order of these two transition states relative to the gas-phase ion chemistry results, while certainly depending on the exact systems examined, might suggest that under proper geometric constraints, such as when confined to a surface, or perhaps more generally in disilene (a compound with a Si═Si bond) chemistry, front-side nucleophilic substitution reactions can be favored over backside attacks. This might have stereochemical implications for certain S_N2 reactions, since the backside attack results in inversion around the carbon center attacked. However, in the case of silicon surface dimers, proton transfer reactions should dominate for alcohols, and the other reaction channels described above are likely to play only a minor role in the surface chemistry of these molecules.

B. Auger Spectroscopy. Figure 6 shows the uptake of 1-propanol on the room temperature Si(100) surface as a function of dose. The uptake was monitored by observing the AES carbon KVV peak intensity at an electron kinetic energy (eKE) of 272 eV. Plots for ethanol and methanol are very similar in appearance and are not shown. From this figure, it can be seen that the initial uptake of propanol on Si(100) rises rapidly until a dose of about 0.5 L. Above this dose level, the carbon Auger signal remains approximately constant and it appears that further propanol is not adsorbed on the surface. The coverage

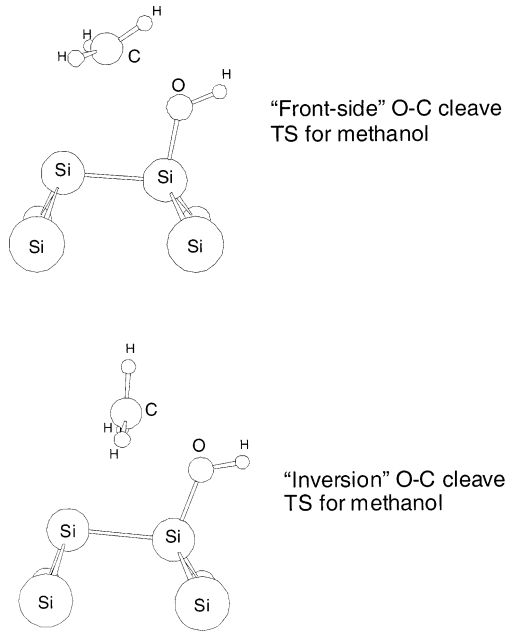

Figure 5. Relative geometries of the "front-side attack" (top) vs "inversion" (bottom) transition states for methyl group transfer during O−C bond cleavage after methanol adsorption onto the Si_9H_{12} cluster. These geometries are the results of the computations described in Section II of the text.

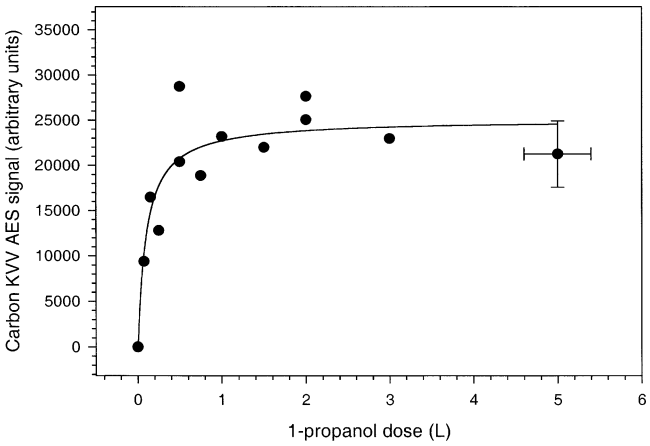

Figure 6. Plot showing the C (KVV) AES peak intensity as a function of 1-propanol dose. The line through the data is a Langmuir adsorption isotherm and is meant only as a guide for the eye.

at and above this 0.5-L dose level can thus be thought of as the saturation coverage of 1-propanol on the Si(100) surface. The ethanol and methanol signals saturate at similar dose levels. To help quantify the alcohol saturation coverages, the carbon AES signal was calibrated with respect to the AES intensity of a saturated layer of methyl iodide (CH_3I) on the Si(100) surface. The carbon AES signal for 1-propanol saturates at 2.86 ± 0.60 times the signal level for a saturation dose of CH_3I, while the signals for ethanol and methanol saturate at 1.95 ± 0.45 and 1.05 ± 0.29 times the CH_3I signal, respectively. Methyl iodide has a room-temperature saturation coverage of 0.43 ± 0.04 monolayers [ML, where 1 ML $= 6.78 \times 10^{14}$ atoms/cm^2 on the Si(100) surface],[61] which indicates that the saturation coverage for 1-propanol is 0.41 ± 0.09 ML on this surface, while ethanol and methanol have coverages of 0.42 ± 0.10 and 0.45 ± 0.13 ML, respectively, on the basis of this comparison. Oxygen Auger signal levels (at 503-eV eKE) showed a similar trend in relative coverage when calibrated with water adsorption,[39] but were weaker in intensity and are not shown.

Saturation coverages of 0.41 to 0.45 ML for these alcohols imply that there is roughly one molecule adsorbed for every two silicon surface atoms (or one molecule per surface dimer), consistent with the picture that emerged from the computational results discussed in Section III.A. The small decrease in observed coverage with increasing chain length (from 0.45 to 0.41 ML) may be due to steric and/or packing effects of these molecules on the Si(100) surface. However, this small decrease may also be due to some screening of the methylene Auger electrons by the outer methyl groups in the case of ethanol and 1-propanol, when compared to methyl iodide and methanol. It is also possible that there is still a small amount of uptake in the high dose region where the Auger signal appears to be saturated in Figure 6, and that very large doses of any of these alcohols could drive the room-temperature saturation coverage closer to a value of 0.5 ML, which would be the theoretical limit of one molecule per surface dimer. An alternative explanation for this slight decrease in coverage for the longer chain alcohols might be that propylene or ethylene formation via β-C−H bond cleavage (see Section III.A, above) can occur at room temperature during dosing. This would lead to a decreasing carbon Auger signal as the barrier to alkene formation out of the datively bonded well decreases. However, the oxygen Auger signal would not be affected by this reaction path, and a detailed comparison of these two signals as a function of dose would reveal whether this channel is an important one for alcohol adsorption. Within our current experimental signal-to-noise, the propanol carbon-to-oxygen AES signal ratio is three times the methanol carbon-to-oxygen ratio, which indicates that, at best, adsorption via the β-C−H bond cleavage channel plays a minor role in the room-temperature adsorption of propanol. In any case, the overall decreases in coverage with increasing chain length are small, and any differences are well within our experimental uncertainties.

Low-energy electron diffraction from the room-temperature surface after administering a 2-L dose of 1-propanol shows a weak two-domain (2×1) reconstructed pattern. Methanol- and ethanol-saturated Si(100) surfaces also show this pattern. While these diffraction patterns are consistent with the $\sim^1/_2$ML coverages obtained by AES, the alcohol overlayers may not be strongly ordered at room temperature and may not provide a noticeable pattern on top of the diffraction from the underlying, strongly ordered silicon surface. While the exact geometry of the alcohol adlayers is not readily apparent from the LEED data, the two-domain (2×1) LEED patterns do indicate that the underlying silicon dimer σ-bonds are intact after alcohol adsorption at room temperature, consistent with alcohol adsorption by either dative bond formation or by an O−H addition reaction.

C. Thermal Desorption. The major thermal desorption peaks observed after room-temperature adsorption of 1-propanol on Si(100) occur at $m/e = 58$, 44, 42, 26, and 2. Several other products (notably $m/e = 28$) can be seen in the thermal desorption traces; however, these all appear to be ionization-induced cracking fragments of the listed major desorption products. Figure 7 shows a typical desorption trace for these major products. It is interesting to note that no parent ($m/e = 60$) desorption channel is observed for this molecule. The heaviest observed product, with $m/e = 58$, has a peak desorption temperature of 670 ± 20 K, and is likely to be due to desorption of propanal (CH_3CH_2CHO). This species is a likely product of a hydrogen elimination reaction of a surface-bound CH_3CH_2-CH_2O species, similar to the production of imines from surface-bound amido radicals[33] and to the production of ethylene from

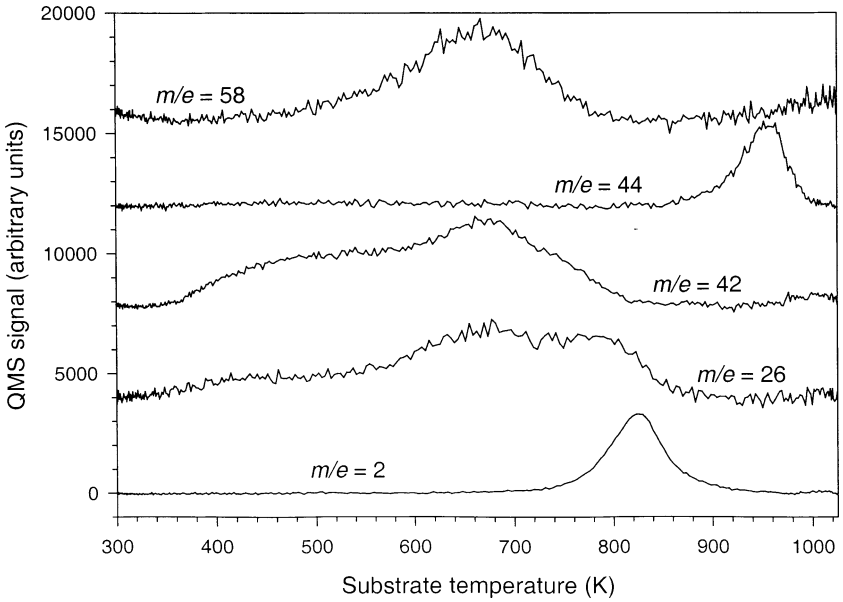

Figure 7. Plot showing the major desorption products from the thermal desorption of a saturation dose of 1-propanol adsorbed at room temperature on the Si(100)−(2 × 1) surface. The mass spectral traces have all been background corrected in this figure.

surface-bound ethyl groups.[62−68] These hydrogen elimination reactions all seem to occur in the 600−700 K temperature range for these species on the Si(100) surface,[33,62−68] consistent with the observed temperature for propanal desorption. The m/e = 44 product has a peak desorption temperature of about 955 K, and is due to SiO desorption. Silicon monoxide desorption products have been previously observed after adsorption of either oxygen[69] or water[39] onto this surface. The m/e = 42 species displays two peaks in the thermal desorption trace, a broad peak at about 485 K and a peak centered at about 670 K. The latter is due to ionization-induced cracking of the m/e = 58 species in the ionizing region of the QMS, while the former appears to be due to a propylene ($CH_3CH{=}CH_2$) desorption channel, possibly related to the propylene desorption channel discussed in Section III.A, or one very similar in nature. The m/e = 26 product appears to display three desorption peaks in this thermal desorption trace, one at about 485 K, one at about 670 K, and one at about 795 K. These first two peaks appear to be ionization-induced cracking fragments, while the highest temperature peak is probably the result of a C_2H_x desorption channel. Similar desorption channels have been observed after adsorption of various carbon-containing species on this surface.[30,61,70] The final major product, with m/e = 2, has a peak desorption temperature of about 825 K and is due to desorption of molecular hydrogen from this surface. The peak desorption temperature for this species is very similar to that observed for the desorption of H_2 after dosing water onto this surface.[39]

To gain further insight into the decomposition reactions observed for 1-propanol on this surface, the thermal desorption of ethanol was also examined. After room-temperature adsorption of a saturation dose of ethanol on the Si(100) surface, thermal desorption revealed four major desorption products having m/e = 44, 28, 26, and 2. Figure 8 shows a sample thermal desorption trace of these species. As was the case with 1-propanol, no ethanol parent (m/e = 46) desorption channel is observed after room-temperature adsorption. The m/e = 44 desorption trace reveals two products having peak desorption temperatures at 630 and 960 K. The higher temperature m/e = 44 peak is due to SiO desorption, as is observed for 1-propanol. The lower temperature peak is likely to be due to desorption of acetaldehyde (CH_3CHO), formed from a hydrogen elimination reaction from a surface-bound ethoxy group, similar to the

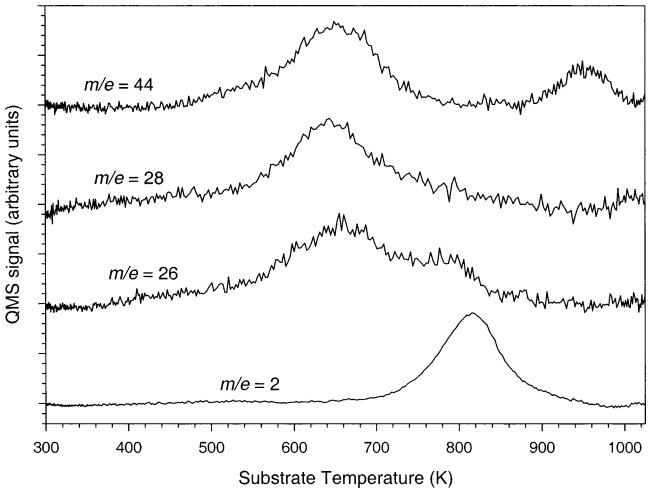

Figure 8. Plot showing the major desorption products from the thermal desorption of a saturation dose of ethanol adsorbed at room temperature on the Si(100)−(2 × 1) surface. The mass spectral traces have all been background corrected in this figure.

mechanism for propanal production as mentioned above. Both the m/e = 28 and 26 peaks appear to be caused by ionization-induced cracking of the lower temperature m/e = 44 peak, although the m/e = 26 trace also seems to have a slightly higher temperature peak at about 790 K. This is very similar in appearance to the m/e = 26 trace observed for propanol and is likely produced by a similar mechanism. The other major product resulting from thermal desorption of ethanol is molecular hydrogen, which has a peak desorption temperature of 815 K in this case.

Thermal desorption from a Si(100) surface saturated with methanol reveals a similar product distribution. Major desorption products are observed at m/e = 44, 30, 28, 16, and 2, as is shown in Figure 9, along with several other ionization-induced cracking products (most notably m/e = 29). Once again, no parent (m/e = 32) desorption channel is observed for methanol. The m/e = 44 product has a peak desorption temperature of about 960 K, and is due to SiO desorption. The m/e = 30 product, which has a peak desorption temperature of about 655 K, appears to be formaldehyde (HCHO), formed from a

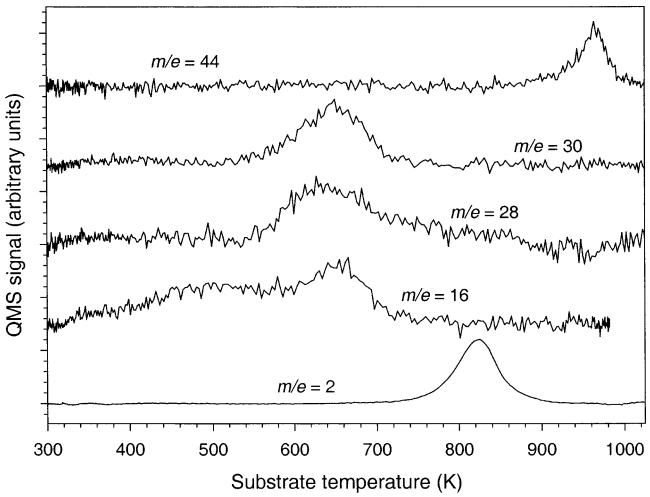

Figure 9. Plot showing the major desorption products from the thermal desorption of a saturation dose of methanol adsorbed at room temperature on the Si(100)−(2 × 1) surface. The mass spectral traces have all been background corrected in this figure.

hydrogen elimination reaction of a surface-bound methoxy species (analogous to the formation of acetaldehyde and propanal mentioned above). The $m/e = 28$ product appears to be an ionization-induced cracking product from formaldehyde and the $m/e = 16$ product seems to have two desorption channels, one at about 525 K, and another at about 655 K, which is likely an ionization-induced cracking product. The identity of the lower temperature $m/e = 16$ desorption product is not entirely clear, and could be due to methane desorption. Investigation into this desorption channel is ongoing. The molecular hydrogen desorption channel ($m/e = 2$) appears at about 830 K.

One general trend observed for the thermal desorption of these three primary alcohols adsorbed on room-temperature Si(100) surfaces is the lack of a parent desorption channel. This is consistent with the computational results outlined in Section III.A that show a small barrier to O−H bond cleavage after the initial physisorption reaction. This can be contrasted to the case of primary and secondary amines, which are predicted to have a more stable (i.e., deeper) physisorbed, dative-bond well,[31−33] and for which a small parent desorption channel due to trapping in this well has been observed.[33] This is also consistent with thermal desorption studies of water adsorbed on this surface, which show no parent desorption from a datively bonded state after room-temperature adsorption.[39] Ammonia shows a parent recombinative desorption channel following adsorption via N−H bond cleavage that competes with decomposition during heating.[25] This recombination channel appears to be suppressed, although still weakly present, once carbon-containing groups are bonded to the nitrogen, as in the case of primary and secondary amines.[33] Water, however, shows no parent recombination desorption channel following adsorption on this surface via O−H cleavage.[39] This is probably due to the predicted −247 kJ/mol depth of the O−H cleavage well (resulting in HOSiSiH surface species),[22] as compared to the shallower (−193 kJ/mol) N−H cleavage well in ammonia (resulting in H_2NSiSiH surface species).[25] The extra stabilization of the oxygen−silicon bond relative to the nitrogen−silicon bond appears to close down the recombination channel, consistent with the lack of any observed alcohol parent recombination products for the primary alcohols examined in this study.

A second general trend in these desorption studies is the observation of the dehydrogenation desorption channel for all of these alcohols. The peak desorption temperatures of these aldehyde products are all in the 630−670 K temperature range, very similar to the imine desorption channel observed after room-temperature adsorption of primary and secondary amines onto this surface.[33] This is also very similar to the temperature range for ethylene production from ethyl halides adsorbed on this surface,[62,65,67,68] which has been shown to proceed via a β-hydrogen elimination reaction of a surface-bound ethyl group formed from dissociative adsorption via C−X bond cleavage. Alcohols are likely to initially undergo O−H bond cleavage upon adsorption, resulting in alkoxy radicals bound to surface silicon atoms. These alkoxy radicals then seem to undergo a similar β-hydrogen elimination reaction to produce aldehydes and hydrogen, which is also observed as a desorption product. For ethyl iodide adsorption on silicon, the ethylene desorption appears to effectively remove all of the carbon-containing species from the surface.[68] This does not appear to be the case for surface-bound alkoxy or amido radicals, however. Amines were observed to have competing surface decomposition and desorption reactions,[33] and the alcohols studied here also displayed evidence for competing desorption channels, both for hydrocarbon desorption ($m/e = 42$ and 26 for 1-propanol, $m/e = 26$ for ethanol, and $m/e = 16$ for methanol) and for silicon monoxide desorption. These channels imply that C−O bond cleavage occurs at some point prior to the desorption of these species, although the exact mechanism for this reaction is unclear at this point. Some of this C−O bond cleavage could occur during the initial, room-temperature adsorption process, although the computational results presented in Section III.A, above, suggest that the majority of adsorption should occur through O−H bond cleavage, resulting in surface-bound alkoxy radicals and hydrogen. This is consistent with previous studies of methanol[15−18] and ethanol[19,20] adsorption on this surface, and appears to apply to 1-propanol as well.

IV. Conclusions

The adsorption of several simple primary alcohols on the Si(100)−(2 × 1) surface has been investigated using Auger electron spectroscopy (AES) and thermal desorption spectroscopy. These molecules appear to undergo dissociative adsorption on this surface at room temperature. The major desorbing thermal decomposition product for all of these species seems to come from β-hydrogen elimination of a surface-bound alkoxy radical to form an aldehyde, a reaction analogous to the formation of ethylene from surface-bound ethyl groups,[62−68] or imines from surface-bound amido radicals.[33] This also results in formation of molecular hydrogen, the other main desorbing product observed for these species. By comparison to the AES results from the adsorption of methyl iodide on Si(100), it was concluded that the initial surface saturation coverage of 1-propanol on Si(100) is slightly less than half a monolayer, identical (within experimental uncertainty) to the saturation coverages of ethanol and methanol. Ab initio and density functional calculations indicate that the O−H cleavage channel is likely the initial adsorption pathway and that very little parent alcohol should be trapped in the molecular physisorbed well upon room-temperature adsorption. This is in good agreement with the experimental results, which provide no evidence for a parent thermal desorption channel, in contrast to experiments on amines,[33] which show a small amount of parent trapping in the deeper nitrogen physisorption well.

Acknowledgment. Acknowledgment is made to the University of Nevada, Reno, for partial support of this research.

Additional financial support from the National Science Foundation is gratefully acknowledged under NSF CAREER Award CHE-0094311.

References and Notes

(1) Waltenburg, H. N.; Yates, J. T. *Chem. Rev.* **1995**, *95*, 1589−1673.
(2) Hamers, R. J.; Wang, Y. J. *Chem. Rev.* **1996**, *96*, 1261−1290.
(3) Wolkow, R. A. *Annu. Rev. Phys. Chem.* **1999**, *50*, 413−441.
(4) Hamers, R. J.; Coulter, S. K.; Ellison, M. D.; Hovis, J. S.; Padowitz, D. F.; Schwartz, M. P.; Greenlief, C. M.; Russell, J. N. *Acc. Chem. Res.* **2000**, *33*, 617−624.
(5) Bent, S. F. *Surf. Sci.* **2002**, *500*, 879−903.
(6) Buriak, J. M. *Chem. Rev.* **2002**, *102*, 1271−1308.
(7) Bent, S. F. *J. Phys. Chem. B* **2002**, *106*, 2830−2842.
(8) Chadi, D. J. *Phys. Rev. Lett.* **1979**, *43*, 43−47.
(9) Hamers, R. J.; Tromp, R. M.; Demuth, J. E. *Phys. Rev. B* **1986**, *34*, 5343−5357.
(10) Boland, J. J. *Adv. Phys.* **1993**, *42*, 129−171.
(11) Duke, C. B. *Chem. Rev.* **1996**, *96*, 1237−1259.
(12) Johnson, A. L.; Walczak, M. M.; Madey, T. E. *Langmuir* **1988**, *4*, 277−282.
(13) Craig, B. I.; Smith, O. V. *Surf. Sci.* **1992**, *262*, 235−244.
(14) Gao, Q.; Cheng, C. C.; Chen, P. J.; Choyke, W. J.; Yates, J. T. *Thin Solid Films* **1993**, *225*, 140−144.
(15) Ehrley, W.; Butz, R.; Mantl, S. *Surf. Sci.* **1991**, *248*, 193−200.
(16) Lu, X.; Zhang, Q.; Lin, M. C. *Phys. Chem. Chem. Phys.* **2001**, *3*, 2156−2161.
(17) Kato, T.; Kang, S.-Y.; Xu, X.; Yamabe, T. *J. Phys. Chem. B* **2001**, *105*, 10340−10347.
(18) Casaletto, M. P.; Zanoni, R.; Carbone, M.; Piancastelli, M. N.; Aballe, L.; Weiss, K.; Horn, K. *Surf. Sci.* **2002**, *505*, 251−259.
(19) Eng, J.; Raghavachari, K.; Struck, L. M.; Chabal, Y. J.; Bent, B. E.; Flynn, G. W.; Christman, S. B.; Chaban, E. E.; Williams, G. P.; Radermacher, K.; Mantl, S. *J. Chem. Phys.* **1997**, *106*, 9889−9898.
(20) Casaletto, M. P.; Zanoni, R.; Carbone, M.; Piancastelli, M. N.; Aballe, L.; Weiss, K.; Horn, K. *Surf. Sci.* **2000**, *447*, 237−244.
(21) Chabal, Y. J. *Surf. Sci. Rep.* **1988**, *8*, 211−357.
(22) Konecny, R.; Doren, D. J. *J. Chem. Phys.* **1997**, *106*, 2426−2435.
(23) Niwano, M.; Terashi, M.; Shinohara, M.; Shoji, D.; Miyamoto, N. *Surf. Sci.* **1998**, *401*, 364−370.
(24) Weldon, M. K.; Queeney, K. T.; Gurevich, A. B.; Stefanov, B. B.; Chabal, Y. J.; Raghavachari, K. *J. Chem. Phys.* **2000**, *113*, 2440−2446.
(25) Dresser, M. J.; Taylor, P. A.; Wallace, R. M.; Choyke, W. J.; Yates, J. T. *Surf. Sci.* **1989**, *218*, 75−107.
(26) Fujisawa, M.; Taguchi, Y.; Kuwahara, Y.; Onchi, M.; Nishijima, M. *Phys. Rev. B* **1989**, *39*, 12918−12920.
(27) Larsson, C. U. S.; Flodstrom, A. S. *Surf. Sci.* **1991**, *241*, 353−356.
(28) Franco, N.; Avila, J.; Davila, M. E.; Asensio, M. C.; Woodruff, D. P.; Schaff, O. V.; Fernandez, V.; Schindler, K.-M.; Bradshaw, A. M. *J. Phys.: Condens. Matter* **1997**, *9*, 8419−8432.
(29) Widjaja, Y.; Mysinger, M. M.; Musgrave, C. B. *J. Phys. Chem. B* **2000**, *104*, 2527−2533.
(30) Mulcahy, C. P. A.; Carman, A. J.; Casey, S. M. *Surf. Sci.* **2000**, *459*, 1−13.
(31) Mui, C.; Wang, G. T.; Bent, S. F.; Musgrave, C. B. *J. Chem. Phys.* **2001**, *114*, 10170−10180.
(32) Cao, X.; Hamers, R. J. *J. Am. Chem. Soc.* **2001**, *123*, 10988−10996.
(33) Carman, A. J.; Zhang, L.; Liswood, J. L.; Casey, S. M. *J. Phys. Chem. B* **2003**, *107*, 5491−5502.
(34) Colaianni, M. L.; Chen, P. J.; Yates, J. T. *J. Vac. Sci. Technol. A* **1994**, *12*, 2995−2998.
(35) Shan, J.; Wang, Y.; Hamers, R. J. *J. Phys. Chem.* **1996**, *100*, 4961−4969.
(36) Miotto, R.; Srivastava, G. P.; Miwa, R. H.; Ferraz, A. C. *J. Chem. Phys.* **2001**, *114*, 9549−9556.
(37) Hohenberg, P.; Kohn, W. *Phys. Rev.* **1964**, *136*, B864−B871.
(38) Kohn, W.; Sham, L. J. *Phys. Rev.* **1965**, *140*, A1133−A1138.
(39) Flowers, M. C.; Jonathan, N. B. H.; Morris, A.; Wright, S. *Surf. Sci.* **1996**, *351*, 87−102.
(40) Kiskinova, M.; Yates, J. T. *Surf. Sci.* **1995**, *325*, 1−10.
(41) Redondo, A.; Goddard, W. A. *J. Vac. Sci. Technol.* **1982**, *21*, 344−350.
(42) Roothaan, C. C. J. *Rev. Mod. Phys.* **1951**, *23*, 69−89.
(43) Frisch, M. J.; Trucks, G. W.; Schlegel, H. B.; Scuseria, G. E.; Robb, M. A.; Cheeseman, J. R.; Zakrzewski, V. G.; Montgomery, J. A.; Stratmann, R. E.; Burant, J. C.; Dapprich, S.; Millam, J. M.; Daniels, A. D.; Kudin, K. N.; Strain, M. C.; Farkas, O.; Tomasi, J.; Barone, V.; Cossi, M.; Cammi, R.; Mennucci, B.; Pomelli, C.; Adamo, C.; Clifford, S.; Ochterski, J.; Petersson, G. A.; Ayala, P. Y.; Cui, Q.; Morokuma, K.; Salvador, P.; Dannenberg, J. J.; Malick, D. K.; Rabuck, A. D.; Raghavachari, K.; Foresman, J. B.; Cioslowski, J.; Ortiz, J. V.; Baboul, A. G.; Stefanov, B. B.; Liu, G.; Liashenko, A.; Piskorz, P.; Komaromi, I.; Gomperts, R.; Martin, R. L.; Fox, D. J.; Keith, T.; Al-Laham, M. A.; Peng, C. Y.; Nanayakkara, A.; Challacombe, M.; Gill, P. M. W.; Johnson, B.; Chen, W.; Wong, M. W.; Andres, J. L.; Gonzalez, C.; Head-Gordon, M.; Replogle, E. S.; Pople, J. A. *Gaussian 98*, Revision A.11; Gaussian, Inc.: Pittsburgh, PA, 2001.
(44) Binkley, J. S.; Pople, J. A.; Hehre, W. J. *J. Am. Chem. Soc.* **1980**, *102*, 939−947.
(45) Gordon, M. S.; Binkley, J. S.; Pople, J. A.; Pietro, W. J.; Hehre, W. J. *J. Am. Chem. Soc.* **1982**, *104*, 2797−2803.
(46) Pietro, W. J.; Francl, M. M.; Hehre, W. J.; Defrees, D. J.; Pople, J. A.; Binkley, J. S. *J. Am. Chem. Soc.* **1982**, *104*, 5039−5048.
(47) Hehre, W. J.; Ditchfield, R.; Pople, J. A. *J. Chem. Phys.* **1972**, *56*, 2257−2261.
(48) Gordon, M. S. *Chem. Phys. Lett.* **1980**, *76*, 163−168.
(49) Pople, J. A.; Krishnan, R.; Schlegel, H. B.; Binkley, J. S. *Int. J. Quantum Chem. Symp.* **1979**, *13*, 225−241.
(50) Johnson, B. G.; Frisch, M. J. *J. Chem. Phys.* **1994**, *100*, 7429−7442.
(51) Gonzalez, C.; Schlegel, H. B. *J. Chem. Phys.* **1989**, *90*, 2154−2161.
(52) Gonzalez, C.; Schlegel, H. B. *J. Phys. Chem.* **1990**, *94*, 5523−5527.
(53) Becke, A. D. *J. Chem. Phys.* **1993**, *98*, 5648−5652.
(54) Lee, C.; Yang, W.; Parr, R. G. *Phys. Rev. B* **1988**, *37*, 785−789.
(55) McLean, A. D.; Chandler, G. S. *J. Chem. Phys.* **1980**, *72*, 5639−5648.
(56) Krishnan, R.; Binkley, J. S.; Seeger, R.; Pople, J. A. *J. Chem. Phys.* **1980**, *72*, 650−654.
(57) Frisch, M. J.; Pople, J. A.; Binkley, J. S. *J. Chem. Phys.* **1984**, *80*, 3265−3269.
(58) Table 1 shows that the methanol O−H cleavage transition state is actually lower in energy than the datively bonded state, at this level of computational treatment. This is due to the differing zero-point vibrational energy corrections applied to the single-point energies. The nonzero-point corrected energies show the datively bonded well slightly below the transition state.
(59) Mui, C.; Han, J. H.; Wang, G. T.; Musgrave, C. B.; Bent, S. F. *J. Am. Chem. Soc.* **2002**, *124*, 4027−4038.
(60) Angel, L. A.; Ervin, K. M. *J. Phys. Chem. A* **2001**, *105*, 4042−4051.
(61) Gutleben, H.; Lucas, S. R.; Cheng, C. C.; Choyke, W. J.; Yates, J. T. *Surf. Sci.* **1991**, *257*, 146−156.
(62) Keeling, L. A.; Chen, L.; Greenlief, C. M.; Mahajan, A.; Bonser, D. *Chem. Phys. Lett.* **1994**, *217*, 136−141.
(63) Darlington, B.; Foster, M.; Campion, A. *Surf. Sci.* **1994**, *304*, L407−L412.
(64) Du, W.; Keeling, L. A.; Greenlief, C. M. *J. Vac. Sci. Technol. A* **1994**, *12*, 2281−2286.
(65) Klug, D.-A.; Greenlief, C. M. *J. Vac. Sci. Technol. A* **1996**, *14*, 1826−1831.
(66) Foster, M.; Darlington, B.; Scharff, J.; Campion, A. *Surf. Sci.* **1997**, *375*, 35−44.
(67) Sampson, G. A.; White, J. M.; Ekerdt, J. G. *Surf. Sci.* **1998**, *411*, 163−175.
(68) Bulanin, K. M.; Shah, A. G.; Teplyakov, A. V. *J. Chem. Phys.* **2001**, *115*, 7187−7195.
(69) Engstrom, J. R.; Bonser, D. J.; Nelson, M. M.; Engel, T. *Surf. Sci.* **1991**, *256*, 317−343.
(70) Jackman, R. B.; Chua, L. H.; Foord, J. S. *Surf. Sci.* **1993**, *292*, 47−60.